ELSEVIER

Journal of Alloys and Compounds 441 (2007) 57–61

Journal of ALLOYS AND COMPOUNDS

www.elsevier.com/locate/jallcom

Syntheses and characterization of $Ln_4Yb_{11}Se_{22}$ (Ln = Ce, Sm, Gd)

Danielle L. Gray, Daniel M. Wells, Kwasi Mitchell, Fu Qiang Huang, James A. Ibers *

Department of Chemistry, Northwestern University, Evanston, IL 60208-3113, United States

Received 25 October 2006; received in revised form 4 December 2006; accepted 5 December 2006
Available online 26 January 2007

Abstract

New interlanthanide selenides $Ln_4Yb_{11}Se_{22}$ (Ln = Ce, Sm, Gd) were synthesized from reactions of their constituent elements at 1123 K. These ordered compounds are isostructural with $Ce_4Lu_{11}S_{22}$, crystallizing with two formula units in the monoclinic space group *C*2/*m*. The structure consists of a network of six- and seven-coordinate Yb atoms penetrated by Ln_2Se_{13} infinite chains. $Gd_4Yb_{11}Se_{22}$ has an antiferromagnetic transition at $T_N = 2.29$ K. $Gd_4Yb_{11}Se_{22}$ is a semiconductor with a resistivity of 103 Ω cm at 298 K.

Keywords: Interlanthanide selenide; Magnetism; Synthesis; X-ray structure

1. Introduction

The interlanthanide chalcogenides show diverse stoichiometries and structural chemistry. Examples include $LnLn'S_3$ (Ln = La–Nd; Ln′ = Y, Dy–Lu) [1–7], $LnYbSe_3$ (Ln = La–Sm) [8], $Ln_3Ln'S_6$ (Ln = La–Sm, Gd; Ln′ = Y, Dy–Lu) [9,10], $La_{10}Er_9S_{27}$ [11], $EuLn_2Q_4$ (Ln = Sc, Y, Tb–Lu; Q = S, Se) [12], $Ln_4Ln'_{11}S_{22}$ (Ln = La, Nd, Sm; Ln′ = Y, Dy–Lu) [13,14], and $LnErTe_2$ (Ln = Tb, Dy) [15]. Most of these compounds are sulfides. These compounds may also show diverse physical properties, but these have been minimally investigated, being limited to the magnetic susceptibilities of $ErLn_2Q_4$ [12], β-$LaYbS_3$, $LnYbSe_3$ (Ln = La, Ce, Pr, Nd, Sm) [8], and the magnetic and optical properties of some $LnLn'S_3$ compounds [7].

Here we report the syntheses and structure of $Ln_4Yb_{11}Se_{22}$ (Ln = Ce, Sm, Gd) together with the magnetic susceptibility and electrical resistivity of $Gd_4Yb_{11}Se_{22}$.

2. Experimental

2.1. Syntheses

Ce (Cerac, 99.9%), Sm (Aldrich, 99.9%), Gd (Strem, 99.9%), Yb (Alfa Aesar, 99.9%), Se (Cerac, 99.999%), and KI (Aldrich, 99%) were used as received. $Ln_4Yb_{11}Se_{22}$ was prepared from the reaction of 0.25 mmol Ln, 0.75 mmol Yb, and 1.5 mmol Se with the addition of approximately 400 mg of KI as flux. Reaction mixtures were loaded into carbon-coated fused-silica tubes under an Ar atmosphere in a glove box. The tubes were then evacuated to 10^{-4} Torr, flame sealed, and placed in a computer-controlled furnace. The reactants for preparation of $Ce_4Yb_{11}Se_{22}$ and $Sm_4Yb_{11}Se_{22}$ were heated to 1123 K in 24 h, kept at 1123 K for 120 h, and rapidly cooled at 69 K/h to 298 K. For $Gd_4Yb_{11}Se_{22}$, the reactants were heated to 1123 K in 15 h, kept at 1123 K for 72 h, cooled at 3.3 K/h to 473 K, and then the furnace was turned off. The products were washed free of flux with water and dried with acetone. Black needles of $Ce_4Yb_{11}Se_{22}$ and $Gd_4Yb_{11}Se_{22}$ and brown needles of $Sm_4Yb_{11}Se_{22}$ were obtained in approximately 70% yield. The compounds are air stable.

2.2. EDX analyses

Energy-dispersive X-ray (EDX) semi-quantitative analyses on selected single crystals were carried out with the use of an Hitachi S-3500 SEM. Data were collected with an accelerating voltage of 20 kV, a working distance of 15 mm, and a collection time of 60 s. Found: Ln:Yb:Se 1:3:6. There was no evidence for other elements with Z > 10, in particular K or I.

2.3. Crystallographic details

Single-crystal X-ray diffraction data were collected with the use of graphite-monochromatized Mo Kα radiation (λ = 0.71073 Å) at 153 K on a Bruker Smart-1000 CCD diffractometer [16]. The crystal-to-detector distance was 5.023 cm. Crystal decay was monitored by re-collecting 50 initial frames at the end of each data collection. For $Gd_4Yb_{11}Se_{22}$, data were collected by a scan of 0.25° in ω in groups of 727 frames at φ settings of 0°, 90°, 180°, and 270°. The exposure time was 10 s/frame. For $Ce_4Yb_{11}Se_{22}$ and $Sm_4Yb_{11}Se_{22}$, data were collected by a scan of 0.3° in ω in groups of 606 frames at φ settings of 0°, 90°, 180°, and 270°. The exposure time was 15 s/frame. The collection of intensity data was carried out with the program SMART [16]. Cell refinement and data reduction were carried out with the use of the program SAINT [16]. A Leitz microscope with a calibrated traveling eyepiece was employed to measure the crystal dimensions

* Corresponding author. Fax: +1 847 491 2976.
E-mail address: ibers@chem.northwestern.edu (J.A. Ibers).

0925-8388/$ – see front matter © 2006 Elsevier B.V. All rights reserved.
doi:10.1016/j.jallcom.2006.12.015

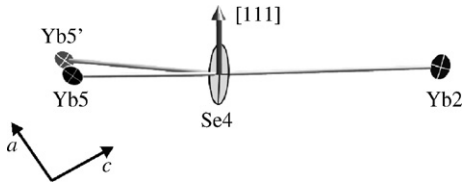

Fig. 1. A representative elongated displacement ellipsoid for atom Se(4) at the 99% probability level as viewed parallel with [1 1 1]. Yb5′ is related to Yb5 by the translation 0, $1 + y_{Yb5}$, 0.

for the face-indexed absorption corrections. These were performed numerically with the use of the program XPREP [17]. Then the program SADABS [16] was employed to make incident beam and decay corrections.

The structures were solved with the direct methods program SHELXS [17]. The two crystallographically independent Ln positions (Ln = Ce, Sm, or Gd) were distinguished from the six independent Yb positions on the basis of coordination numbers and Ln–Se distances. The structures were refined with the full-matrix least-squares program SHELXL [17]. Initial refinements converged smoothly to values of $R(F)$ of around 0.04 and, with one exception, to sensible anisotropic displacement ellipsoids. Among the two independent Ln atoms, the six independent Yb atoms, and the 11 independent Se atoms, the exception was atom Se(4), which is in the center of a trigonal plane of Yb atoms. For all three structures, it displayed large displacement parameters with elongation in the [1 1 1] direction (Fig. 1). When the Se(4) position was split over two sites the ensuing refinement led to an occupancy of the original site of about 80% and that of the second site of about 20%; the values of $R(F)$ for the Ce, Sm, and Gd structures went from 0.039, 0.042, 0.042 to 0.041, 0.045, 0.040, respectively. Moreover, the displacement ellipsoids remained elongated. Accordingly, the Se(4) position was left as a single site in the final refinements.

The program Structure Tidy [18] was used to standardize the positional parameters of $Ln_4Yb_{11}Se_{22}$ (Ln = Ce, Sm, Gd). Additional experimental details are given in Table 1 and in Appendix A Supporting material. Selected distances are presented in Table 2.

2.4. Magnetic susceptibility measurements of $Gd_4Yb_{11}Se_{22}$

DC magnetic susceptibility measurements on $Gd_4Yb_{11}Se_{22}$ were carried out with the use of a Quantum Design MPMS5 SQUID magnetometer. Nineteen milligrams of ground single crystals were loaded into a gelatin capsule. In the temperature range between 1.8 and 300 K both zero-field-cooled (ZFC) and field-cooled (FC) measurements were made with a 500 G applied field. All data were corrected for electron core diamagnetism [19].

Table 1
Crystal data and structure refinements for $Ln_4Yb_{11}Se_{22}$ (Ln = Ce, Sm, Gd)[a]

	$Ce_4Yb_{11}Se_{22}$	$Sm_4Yb_{11}Se_{22}$	$Gd_4Yb_{11}Se_{22}$
formula mass	4201.04	4241.96	4269.56
a (Å)	40.319(4)	40.237(8)	40.331(3)
b (Å)	4.0667(4)	4.0436(8)	4.0468(2)
c (Å)	11.735(1)	11.713(2)	11.7426(7)
β (degrees)	91.027(3)	91.070(3)	91.058(1)
V (Å^3)	1923.9(3)	1905.4(7)	1916.21(19)
ρ_c (g/cm^3)	7.252	7.394	7.400
μ (cm^{-1})	518.66	537.56	542.45
$R(F)$[b]	0.039	0.042	0.042
$R_w(F^2)$[c]	0.094	0.114	0.108

[a] For all structures space group = $C2/m$, $Z = 2$, $T = 153(2)$ K, and $\lambda = 0.71073$ Å.
[b] $R(F) = \Sigma||F_o| - |F_c||/\Sigma F_o$ for $F_o^2 > 2\sigma(F_o^2)$.
[c] $R_w(F^2) = \{\Sigma[w(F_o^2 - F_c^2)^2]/\Sigma w F_o^4\}^{1/2}$ for all data. $w^{-1} = \sigma^2(F_o^2) + (q \times F_o^2)^2$ for $F_o^2 < 0$ and $w^{-1} = \sigma^2(F_0^2)$ for $F_o^2 < 0$. $q = 0.04$ for $Gd_4Yb_{11}Se_{22}$, and $q = 0.05$ for $Ce_4Yb_{11}Se_{22}$ and $Sm_4Yb_{11}Se_{22}$.

Table 2
Selected distances (Å) for $Ln_4Yb_{11}Se_{22}$ (Ln = Ce, Sm, and Gd)

Distance	$Ce_4Yb_{11}Se_{22}$	$Sm_4Yb_{11}Se_{22}$	$Gd_4Yb_{11}Se_{22}$
Ln1–Se1	3.107(2)	3.076(2)	3.086(2)
Ln1–Se6 × 2	3.140(2)	3.112(2)	3.108(2)
Ln1–Se7 × 2	3.116(2)	3.075(2)	3.069(1)
Ln1–Se8 × 2	3.013(2)	2.971(2)	2.955(1)
Ln1–Se9	3.044(2)	3.004(2)	2.996(2)
Ln2–Se1 × 2	3.003(2)	2.955(2)	2.943(1)
Ln2–Se2 × 2	3.076(1)	3.042(2)	3.031(2)
Ln2–Se5 × 2	3.084(2)	3.054(2)	3.052(2)
Ln2–Se8	3.082(2)	3.052(2)	3.047(2)
Yb1–Se2	2.966(2)	2.978(2)	2.996(2)
Yb1–Se8 × 2	2.958(1)	2.976(2)	2.993(1)
Yb1–Se9	2.842(2)	2.837(2)	2.844(2)
Yb1–Se11 × 2	2.796(1)	2.815(2)	2.824(1)
Yb1–Se11	2.965(2)	2.975(2)	2.976(2)
Yb2–Se1 × 2	2.863(1)	2.869(1)	2.879(1)
Yb2–Se4	2.716(2)	2.705(2)	2.691(2)
Yb2–Se7	2.815(2)	2.813(2)	2.834(2)
Yb2–Se10 × 2	2.789(1)	2.782(2)	2.790(1)
Yb3–Se3	2.789(2)	2.783(2)	2.791(2)
Yb3–Se5 × 2	2.856(1)	2.853(1)	2.866(1)
Yb3–Se6	2.794(2)	2.793(2)	2.806(2)
Yb3–Se9 × 2	2.730(1)	2.730(1)	2.739(1)
Yb4–Se2 × 2	2.836(1)	2.836(1)	2.848(1)
Yb4–Se3 × 2	2.801(1)	2.803(1)	2.812(1)
Yb4–Se3	2.844(2)	2.832(2)	2.838(2)
Yb4–Se11	2.746(2)	2.738(2)	2.747(2)
Yb5–Se4 × 2	2.723(2)	2.723(2)	2.729(2)
Yb5–Se5	2.823(2)	2.833(2)	2.843(2)
Yb5–Se6 × 2	2.853(1)	2.850(1)	2.865(1)
Yb5–Se10	2.827(2)	2.809(2)	2.811(2)
Yb6–Se7 × 4	2.808(1)	2.821(1)	2.845(1)
Yb6–Se10 × 2	2.837(2)	2.838(2)	2.844(2)

2.5. Electrical resistivity measurement of $Gd_4Yb_{11}Se_{22}$

The electrical resistivity along the crystallographic b-axis of a single crystal of $Gd_4Yb_{11}Se_{22}$ was measured between 400 and 2.0 K by standard four-probe ac methods with the use of a Quantum Design PPMS instrument. Four leads constructed of 15 μm diameter Cu wire and 8 μm diameter graphite fibers were attached with DOW 4929N silver paint to a single crystal 626 μm in length.

3. Results

3.1. Syntheses

Ln (Ln = Ce, Sm, Gd), Yb, and Se were reacted in a Ln:Yb:Se ratio of l:3:6 in the presence of excess KI flux at 1123 K in an effort to produce $LnYb_3Se_6$. Instead the reaction afforded high quality crystals of $Ln_4Yb_{11}Se_{22}$ in yields of approximately 70%.

3.2. Crystal structures

The $Ln_4Yb_{11}Se_{22}$ (Ln = Ce, Sm, Gd) compounds are isostructural and have the $Ce_4Yb_{11}S_{22}$ structure type [13], as do the analogous sulfides $Ln_4Ln'_{11}S_{22}$ (Ln = La–Sm; Ln′ = Dy–Lu) [14]. The crystal structure is illustrated in Fig. 2. The structure consists of a network of Ln_2Se_{13} infinite chains that penetrate a YbSe network of $YbSe_6$ and $YbSe_7$ polyhedra. The Ln_2Se_{13} chains consist of two independent Ln atoms with m site symme-

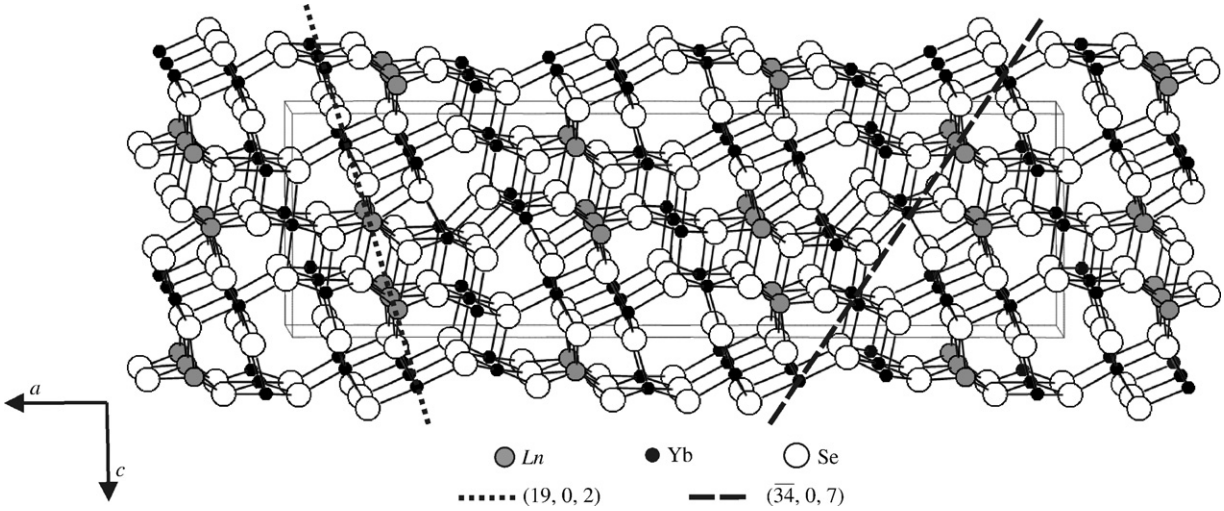

Fig. 2. The structure of $Gd_4Yb_{11}Se_{22}$ as a representative of the $Ln_4Ln'_{11}Q_{22}$ family of compounds.

try. Atom Ln(1) is coordinated by eight Se atoms in a bicapped trigonal prism whereas atom Ln(2) is coordinated by seven Se atoms in a capped trigonal prism. Each Ln(1) prism edge shares with two Ln(2) prisms. Each Ln prism also face shares with two symmetric equivalents to propagate the chain in the [0 1 0] direction (Fig. 3). The YbSe network consists of six independent Yb sites. The Yb(1) atom has *m* symmetry and sits in a $YbSe_7$ capped trigonal prism, as does Ln(2). The remaining five Yb atoms sit in $YbSe_6$ octahedra or distorted octahedra in sites with *m* symmetry except for Yb(6), which sits in a site with 2/*m* symmetry. A structurally similar motif is found in the structure of $CeYb_3S_6$ [9].

In the $Ln_4Yb_{11}Se_{22}$ compounds, the Ln–Se and Yb–Se distances are normal (Table 2). The following comparisons can be made: Ce–Se, 3.003(2)–3.140(2) Å versus 3.018(2)–3.168(2) Å in $KCuCe_2Se_6$ [20]; Sm–Se, 2.955(2)–3.112(2) Å versus 2.8692(11)–3.1705(1) Å in Sm_3CeSe_6 [21]; Gd–Se, 2.943(1)–3.108(2) Å versus 2.847(1)–3.151(1) Å in Gd_3CrSe_6 [21]; Yb–Se, 2.691(2)–2.996(2) Å versus 2.752(3)–2.939(2) Å in $Rb_3Yb_7Se_{12}$ [22]. Although the stereochemistry, the normalcy of the distances, and the generally satisfactory refinements suggest that there is minimal disorder of the rare-earth elements in these compounds, there is no way to quantify this with the use of the present X-ray data. The same statement can, of course, be made for all interlanthanide structures derived from X-ray data collected at standard wavelengths.

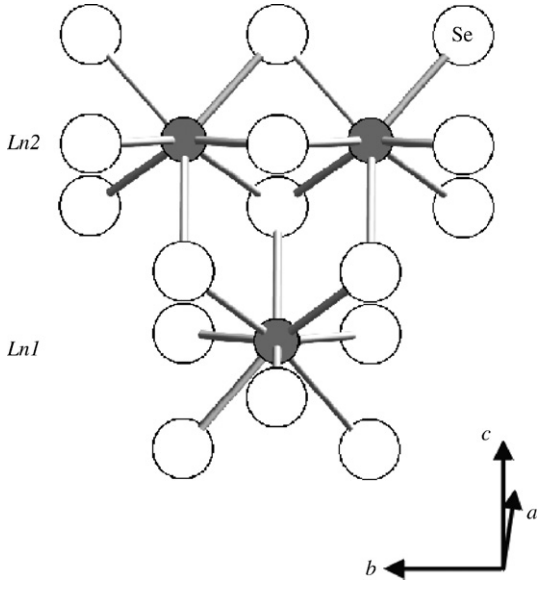

Fig. 3. The Ln_2Se_{13} infinite chain that propagates in the [0 1 0] direction.

3.3. Magnetic susceptibility of $Gd_4Yb_{11}Se_{22}$

The molar magnetic susceptibility χ_m as well as χ_m^{-1} of $Gd_4Yb_{11}Se_{22}$ from 1.8 to 300 K are shown as a function of temperature in Fig. 4. The compound shows Curie–Weiss behavior $\chi_m^{-1} = (T - \theta_p)/C$ between 100 and 300 K, with $\theta_p = -25.1(6)$ K and $C = 62.6(2)$ emu K mol^{-1} for ZFC data and $\theta_p = -31.4(6)$ K and $C = 62.0(3)$ emu K mol^{-1} for FC data. Below 100 K crystal-field effects cause a deviation from Curie–Weiss behavior. ZFC and FC molar magnetic susceptibilities begin to differ increasingly below 5 K. This may occur because of magnetic impurities in the rare earths or because of magnetic frustration among metals over the eight independent rare-earth sites. Views along the planes (19,0,2) and ($\overline{34}$,0,7) and normal to these planes are shown in Figs. 2 and 5, respectively. These views illustrate layers constructed from triangles and squares where magnetic frustration could occur. Despite the dependence of the magnetization on field, the values of T_{max} for ZFC and FC data are identical. There is an ordering transition at $T_N = 2.29$ K, which is presumably antiferromagnetic in view of the negative Weiss constant.

3.4. Electrical resistivity of $Gd_4Yb_{11}Se_{22}$

The electrical resistivity along the *b*-axis of a single crystal of $Gd_4Yb_{11}Se_{22}$ is shown as a function of temperature in Fig. 6.

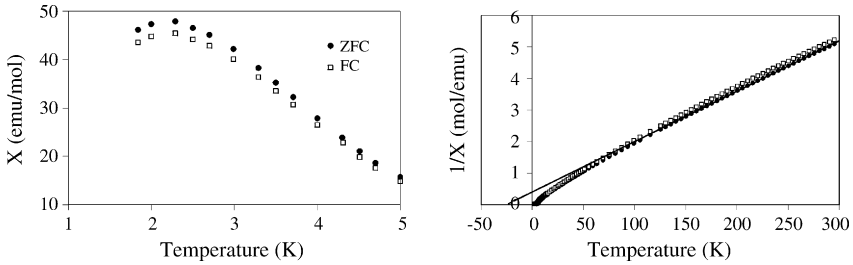

Fig. 4. Molar magnetic susceptibility χ_m and inverse molar magnetic susceptibility χ_m^{-1} vs. T for ZFC and FC data collected on single crystals of $Gd_4Yb_{11}Se_{22}$.

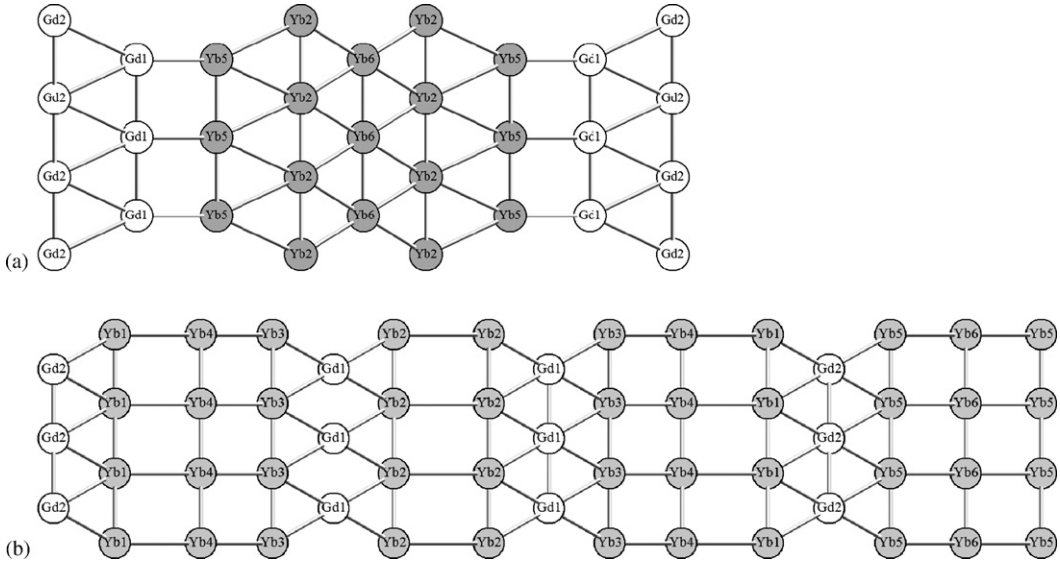

Fig. 5. View of the Gd and Yb layers based on triangles and squares: (a) view of layers parallel to the (19,0,2) plane and (b) view of layers parallel to the ($\overline{34}$,0,7) plane.

The material is a semiconductor with resistivity increasing with decreasing temperature. Below 182 K the resistance is beyond the detection limit of the instrument. The data shown in Fig. 6 lead to an activation energy of 0.14 eV. The material has resistivity of 103 Ω cm at 298 K. Given the three-dimensional nature of the structure it is unlikely that the resistivity behavior in other crystal directions will be greatly different from that along the *b*-axis.

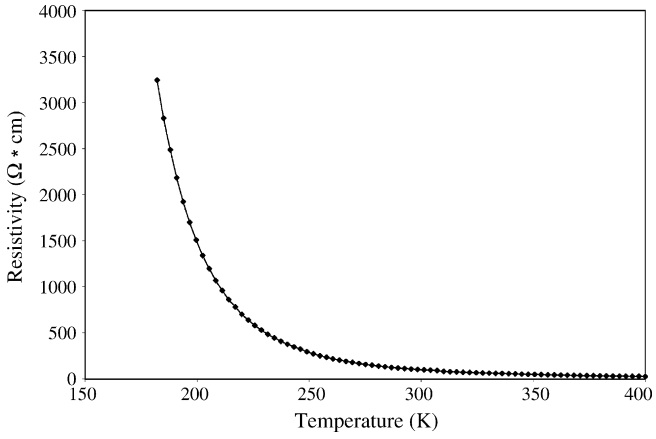

Fig. 6. As a function of temperature the electrical resistivity along the *b*-axis of a single crystal of $Gd_4Yb_{11}Se_{22}$.

4. Discussion

If one assumes that the rare-earth elements are in their 3+ state then the formula $Ln_4Yb_{11}Se_{22}$ presents a problem of charge balance. One either needs more anionic charge or less cationic charge. Greater anionic charge could be achieved if some Se sites were replaced with anions of charge more negative charge than 2−. The carbon-coated Si tubes were not abraded during the reactions that provided the title compounds in good yield. Consequently, anions such as C^{4-} or Si^{4-} can be ruled out. Of course, the EDX results preclude Si^{4-}. N^{3-} can be ruled out because the reactions were carried out in evacuated tubes. Moreover, the X-ray data cannot be satisfied with entities of such low atomic number. The total anionic charge is thus 44−. The value of 44+ is thus required for total cation charge. Because this same charge balance must be achieved for Ln = Ce, Sm, and Gd we presume that these structures contain 10 Yb^{3+} ions and 1 Yb^{2+} ion per formula unit and that these are distributed statistically over the six crystallographically independent Yb sites in the crystal structures. $Gd_4Yb_{11}Se_{22}$ is a semiconductor; presumably $Ce_4Yb_{11}Se_{22}$ and $Sm_4Yb_{11}Se_{22}$ are also. Thus, an alternative way to achieve charge balance is with 11 Yb^{3+} ions and one electron per formula unit in the conduction band.

However, the possibility that the structures contain 14.667 rather than 15.0 rare-earth elements cannot be eliminated.

The displacement parameters for the eight crystallographically independent rare-earth elements in the structures offer no clues. Neither do the magnetic data. From the magnetic susceptibility measurements for the ZFC data the effective magnetic moment μ_{eff} for $Gd_4Yb_{11}Se_{22}$ is 22.4(1) μ_B. Theoretical values are 21.4 μ_B for $Gd_4^{3+}Yb_{10}^{3+}Yb^{2+}Se_{22}$, 21.7 μ_B for $Gd_4^{3+}Yb_{10.667}^{3+}Se_{22}$, 21.4 μ_B for $Gd_{3.67}^{3+}Yb_{11}^{3+}Se_{22}$, and between 21.4 and 21.7 μ_B when there are vacancies on all rare-earth sites.

Acknowledgment

Funding for this work was kindly provided by U.S. Department of Energy BES Grant ER-15522.

Appendix A. Supporting material

The crystallographic files in cif format for $Ce_4Yb_{11}Se_{22}$, $Sm_4Yb_{11}Se_{22}$, and $Gd_4Yb_{11}Se_{22}$ have been deposited with FIZ Karlsruhe as CSD numbers 417138, 417139, and 417137, respectively. These data may be obtained free of charge by contacting FIZ Karlsruhe at +49 7247 808 666 (fax) or crysdata@fix-karlsruhe.de (email).

References

[1] N. Rodier, Bull. Soc. Fr. Mineral. Cristallogr. 96 (1973) 350–355.
[2] D. Carré, P. Laruelle, Acta Crystallogr. Sect. B: Struct. Crystallogr. Cryst. Chem. 30 (1974) 952–954.
[3] N. Rodier, R. Julien, V. Tien, Acta Crystallogr. Sect. C: Cryst. Struct. Commun. 39 (1983) 670–673.
[4] T. Vovan, D. Carré, P. Khodadad, C.R. Seances, Acad. Sci. Ser. C 271 (1970) 1571–1573.
[5] T. Vovan, P. Khodadad, Bull. Soc. Chim. Fr. (1971) 3454–3458.
[6] N. Rodier, V. Tien, C.R. Acad. Sci. Paris 285 (1977) 133–136.
[7] G.B. Jin, E.S. Choi, R.P. Guertin, J.S. Brooks, T.H. Bray, C.H. Booth, T.A.S. Albrecht-Schmitt, private communication.
[8] K. Mitchell, R.C. Somers, F.Q. Huang, J.A. Ibers, J. Solid State Chem. 177 (2004) 709–713.
[9] N. Rodier, V. Tien, C.R. Seances, Acad. Sci. Ser. C 279 (1974) 817–823.
[10] N. Rodier, V. Tien, M. Guittard, Mater. Res. Bull. 11 (1976) 1209–1218.
[11] D. Carré, J. Flahaut, P. Khodadad, P. Laruelle, N. Rodier, V. Tien, J. Solid State Chem. 7 (1973) 321–336.
[12] F. Hulliger, O. Vogt, Phys. Lett. 21 (1966) 138–139.
[13] N. Rodier, V. Tien, Bull. Soc. Fr. Mineral. Cristallogr. 98 (1975) 30–35.
[14] T. Vovan, M. Guittard, N. Rodier, Mater. Res. Bull. 14 (1979) 597–602.
[15] A. Khan, C. García, in: C.E. Lundin (Ed.), Proceedings of the 12th Rare Earth Research Conference, July 18–22, 1976, Vail, Colorado, vol. 2, University of Denver, Denver, 1976, pp. 953–960.
[16] Bruker, SMART Version 5.054 Data Collection and SAINT-Plus Version 6.45a Data Processing Software for the SMART System (Bruker Analytical X-Ray Instruments, Inc., Madison, WI, USA), 2003.
[17] G.M. Sheldrick, SHELXTL Version 6.14 (Bruker Analytical X-Ray Instruments, Inc., Madison, WI, USA), 2003.
[18] L.M. Gelato, E. Parthé, J. Appl. Crystallogr. 20 (1987) 139–143.
[19] L.N. Mulay, E.A. Boudreaux, Theory and Applications of Molecular Diamagnetism, Wiley-Interscience, New York, 1976.
[20] Y. Klawitter, C. Näther, I. Jeβ, W. Bensch, M.G. Kanatzidis, Solid State Sci. 1 (1999) 421–431.
[21] O. Tougait, J.A. Ibers, Inorg. Chem. 39 (2000) 1790–1794.
[22] S.-J. Kim, S.-J. Park, H. Yun, J. Do, Inorg. Chem. 35 (1996) 5283–5289.